Jpn. J. Appl. Phys. Vol. 36 (1997) pp. 5714–5723
Part 1, No. 9A, September 1997

Modeling and Simulation of a Large-Area Plasma Source

Jae Koo LEE, Lin MENG*, Young Kyo SHIN, Hae June LEE and Tae Hun CHUNG[1]

Pohang University of Science and Technology, Pohang 790-784, Korea,
[1]*Dong-A University, Pusan 604-714, Korea*

(Received December 9, 1996; accepted for publication June 30, 1997)

A variant of transformer-coupled plasma, suitable for processing a large-area flat panel with good uniformity, is examined using various models and simulations. Using two-dimensional and one-dimensional fluid simulations, we present the detailed profiles of the plasma density, potential, electron temperature, electric field structure, and ion current density at the substrate. The average values compare reasonably well with those of a global (volume-averaged) model.

KEYWORDS: fluid, simulation, plasma, processing, global, modeling, transformer-coupled

1. Introduction

Glow discharges are widely used in a number of applications such as gas discharge lasers, plasma display panels, high-power switches, and plasma processing.[1–3] A large-area, rf inductively driven plasma source using a variant of a transformer-coupled plasma (TCP) without a magnetic field is under investigation for processing large flat panels with a good uniformity. As the dimension of the antenna coil of an rf-powered plasma system increases and becomes comparable to the rf wavelength, the nonuniformity of the plasma source due to standing waves becomes an important obstacle to overcome. A novel TCP plasma source launching a traveling wave is being developed[4] for processing a large flat area (wafer of 30 cm diameter or 36 by 46.5 cm flat panel) with relatively uniform plasma densities. The schematic of the planar geometry used in experiments is shown in Fig. 1(a), eight antennas launch a traveling wave by a common rf power supply through eight conductors of 1 cm radius which are connected continuously at both ends of the third dimension.

We simulate certain characteristics of the plasma source by using some simplified assumptions. A self-consistent treatment of rf-electromagnetic field in the inductively coupled source is not included in our simple electrostatic fluid simulations. We parametrize the source in terms of a characteristic width and depth. Here, the width is the separation between line sources and the depth is the distance between the planar array and the substrate. The simple modeling analysis carried out elsewhere[5] for calculating the nonuniformity of a planar array of eight line sources reveals that there is an optimum ratio of the width to depth dimensions for minimizing the nonuniformity to less than 5% for the above source and substrate dimensions, as well as for neutral gas pressures ranging from 10 to 100 mTorr.

Fluid models[6–15] for charged particles are widely used as approximation of the general kinetic treatment, and they appear to be useful for the understanding of the physical phenomena of the discharges. The local field equilibrium approximation is often used. The ionization source term is assumed to be a function of E/p, where E is the magnitude of the electric field and p is the gas pressure.

Two-dimensional and one-dimensional fluid-simulation codes[16,17] in Cartesian coordinates have been developed and used to simulate the plasma dynamics of generation and loss. In this work, the equations of continuity of electrons and ions, along with electron energy balance, and Poisson's equation have been dynamically examined to reveal the steady profiles of the densities of electrons and ions and the electron temperature with self-consistent potential. The self-consistent calculation of the induced electric fields, as in some recent work,[18–20] is not included in this simulation in which Poisson's equation is solved in lieu of the Maxwell equations and the induced electric field effects are approximated by the power deposition profile, as specified by Lieberman and Lichtenberg[1] and Stewart *et al.*[21] The calculated uniformity for various plasma quantities is discussed.

This paper is organized in the following manner: the physical model and basic equations are described in §2. The method of solution is given in §3. The results of using two-dimensional and one-dimensional codes along with global modeling are shown in the subsequent sections. Finally, a summary and conclusions follow.

2. Physical Model

The model includes the following assumptions: (1) the electron energy distribution is Maxwellian (the validity of which, in our parameter regime, should be tested in a future study using a kinetic model), (2) the particle motion is collision-dominated, so that the fluid model is valid, (3) the transport parameters, such as mobility and diffusion of charged particles, are functions of E/p, (4) the ionization rate for the discharge is a function of electron temperature, (5) the density and temperature of the neutral gas are constant in the chamber. Under these assumptions, the model equations are written as

$$\frac{\partial n_e}{\partial t} + \nabla \cdot \boldsymbol{\Gamma}_e = R_{iz} - \alpha n_e n_p, \tag{1}$$

$$\frac{\partial n_p}{\partial t} + \nabla \cdot \boldsymbol{\Gamma}_p = R_{iz} - \alpha n_e n_p, \tag{2}$$

$$\frac{\partial}{\partial t}\left(\frac{3}{2} n_e k T_e\right) + \nabla \cdot \boldsymbol{q}_e + e\boldsymbol{\Gamma}_e \cdot \boldsymbol{E}$$

*Permanent address: High Energy Electronics Institute, Universityof Electronic Science and Technology of China, Chengdu, Sichuan 610054, China.

$$+ P_{\text{coll}} = P - \alpha\left(\frac{3}{2}n_e n_p k T_e\right), \quad (3)$$

$$\nabla^2 V = \frac{e}{\epsilon_0}(n_e - n_p), \quad (4)$$

$$\boldsymbol{\Gamma}_e = -D_e \nabla n_e - n_e \mu_e \boldsymbol{E}, \quad (5)$$

$$\boldsymbol{\Gamma}_p = -D_p \nabla n_p + n_p \mu_p \boldsymbol{E}, \quad (6)$$

$$\boldsymbol{q}_e = -\frac{5}{2}n_e D_e \nabla(kT_e) + \frac{5}{2}kT_e \boldsymbol{\Gamma}_e. \quad (7)$$

Here, $n_{e(p)}$, $D_{e(p)}$, and $\mu_{e(p)}$ are the density, diffusion, and mobility of electrons (ions), respectively. V, T_e, k, e, and ϵ_0 are potential, electron temperature, Boltzmann constant, electron charge, and permittivity of free space, respectively. α is the recombination coefficient of the neutral gas (argon) and P is the power density absorbed in the system. P_{coll} is the energy loss rate per volume due to electron-neutral collisions. The ionization rate source term R_{iz} is written in the form given by Stewart *et al.*:[18]

$$R_{\text{iz}} = n_e N K_{\text{iz}}, \quad (8)$$

where N is the density of the neutral gas and K_{iz} is the ionization rate constant. All the densities are in $10^9\,\text{cm}^{-3}$ and R_{iz} is in $10^{18}\,\text{cm}^{-3}\cdot\text{s}^{-1}$. The electron collisional power loss P_{coll} is assumed to be due to the collisional loss due to ionization, excitations, and the elastic energy transfer. It can be expressed by

$$P_{\text{coll}} = n_e N \sum_j K_j \varepsilon_j, \quad (9)$$

where the sum is over the collisional processes, ε_j is the energy loss per collision type j, and the rate constants $K_j(T_e)$ are fitted by the following functional form:

$$K_j(T_e) = \alpha_{1j}\exp(-\alpha_{2j}/T_e), \quad (10)$$

where the constants α_{1j}, α_{2j} and ε_j are as given by Stewart *et al.*[18] for argon.

The diffusion coefficients and mobilities of electron and argon are functions of the reduced field E/p, and are given by[22]

$$D_e p = 1.2 \times 10^6\,\text{cm}^2\cdot\text{s}^{-1}\cdot\text{Torr},$$

$$D_p p = 40\,\text{cm}^2\cdot\text{s}^{-1}\cdot\text{Torr},$$

$$\mu_e p = 3.0 \times 10^5\,\text{cm}^2\cdot\text{V}^{-1}\cdot\text{s}^{-1}\cdot\text{Torr}.$$

The ion mobility is given by[23]

$$\mu_p = 10^3(1\text{–}2.22 \times 10^{-3}E/p)/p \quad \text{cm}^2\cdot\text{V}^{-1}\cdot\text{s}^{-1}$$
$$\text{for} \quad E/p \le 60\,\text{V}\cdot\text{cm}^{-1}\cdot\text{Torr}^{-1},$$

and

$$\mu_p = \frac{8.25 \times 10^3}{p\sqrt{E/p}}[1 - 86.52/(E/p)^{3/2}] \quad \text{cm}^2\cdot\text{V}^{-1}\cdot\text{s}^{-1}$$
$$\text{for} \quad E/p > 60\,\text{V}\cdot\text{cm}^{-1}\cdot\text{Torr}^{-1}.$$

The boundary conditions to solve the above equations are as follows: the voltages and the densities of charge particles on the electrodes and wall are set to zero. The electron temperature on the electrodes and wall is controlled by an input parameter, but usually set to 0.5 eV.[3] The secondary electron emission coefficient is adjustable, but is usually set to zero.

3. Numerical Method

The equations are discretized by the finite difference method for the spatial derivatives, while the time derivatives are discretized by forward time centered space (FTCS). The continuity equations, electron balance equation [$f_{ij} = (n_e k T_e)_{ij}$ has been defined for convenience], and Poisson's equations are discretized by the following FTCS scheme.

$$\frac{n_{ij}^{k+1} - n_{ij}^k}{\Delta t} + \frac{(\Gamma_x)_{i+\frac{1}{2},j}^{k+1} - (\Gamma_x)_{i-\frac{1}{2},j}^{k+1}}{\Delta x} + \frac{(\Gamma_y)_{i,j+\frac{1}{2}}^{k+1} - (\Gamma_y)_{i,j-\frac{1}{2}}^{k+1}}{\Delta y} = (R_{\text{iz}})_{ij}^k \quad (11)$$

$$\frac{3}{2}\frac{f_{ij}^{k+1} - f_{ij}^k}{\Delta t} + \frac{(q_{ex})_{i+\frac{1}{2},j}^{k+1} - (q_{ex})_{i-\frac{1}{2},j}^{k+1}}{\Delta x} + \frac{(q_{ey})_{i,j+\frac{1}{2}}^{k+1} - (q_{ey})_{i,j-\frac{1}{2}}^{k+1}}{\Delta y} = -e(\Gamma_{ex})_{ij}^k (E_x)_{ij}^k - e(\Gamma_{ey})_{ij}^k (E_y)_{ij}^k - P_{\text{coll}} \quad (12)$$

$$\frac{V_{i+1,j}^{k+1} - 2V_{i,j}^{k+1} + V_{i-1,j}^{k+1}}{(\Delta x)^2} + \frac{V_{i,j+1}^{k+1} - 2V_{i,j}^{k+1} + V_{i,j-1}^{k+1}}{(\Delta y)^2} = \frac{e}{\epsilon_0}(n_p - n_e)_{ij}^k \quad (13)$$

The electron energy flux can be rewritten in the form

$$\boldsymbol{q}_e = -\frac{5}{2}D_e \nabla(n_e k T_e) - \frac{5}{2}\mu_e (n_e k T_e)\boldsymbol{E} = -\frac{5}{2}D_e \nabla f - \frac{5}{2}\mu_e f \boldsymbol{E}, \quad (14)$$

This is in the form similar to that for the fluxes of charged particles using the exponential scheme proposed by Sharfetter and Gummel:[24]

$$(\Gamma_x)_{i+\frac{1}{2},j}^{k+1} = \frac{D}{\Delta x}\left[n_{ij}^{k+1}\exp\left(z_{i+\frac{1}{2},j}^k\right) - n_{i+1,j}^{k+1}\right] \times \frac{z_{i+\frac{1}{2},j}^k}{\exp\left(z_{i+\frac{1}{2},j}^k\right) - 1} \quad (15)$$

$$(q_{ex})_{i+\frac{1}{2},j}^{k+1} = \frac{5}{2}\frac{D}{\Delta x}\left[f_{ij}^{k+1}\exp\left(z_{i+\frac{1}{2},j}^k\right) - f_{i+1,j}^{k+1}\right] \times \frac{z_{i+\frac{1}{2},j}^k}{\exp\left(z_{i+\frac{1}{2},j}^k\right) - 1}, \quad (16)$$

where

$$z_{i+\frac{1}{2},j}^k = -s\frac{\mu}{D}(V_{i+1,j}^k - V_{i,j}^k)$$

and $s = +1$ for the positive ions and $s = -1$ for the electrons. Similar expressions can be obtained for y components. The principal advantage of this exponential discretization scheme is that it provides numerical stability of the fluxes under all conditions.

The equations can be written in a matrix form:

$$a_{ij}u_{i+1,j} + b_{ij}u_{i-1,j} + c_{ij}u_{i,j+1} + d_{ij}u_{i,j-1}$$

$$+ e_{ij}u_{ij} = f_{ij}. \quad (17)$$

The obtained algebraic equations are solved by the SOR method until convergent solutions are obtained.

The authors also performed separate calculations using the explicit method (modified two-step Lax-Wendrof method) and alternate direction implicit (ADI) method to solve the continuity equations and the electron energy balance equation; the results are in good agreement with those obtained using the implicit method. The differences between the results of the two methods are less than 0.1%. The implicit scheme is more efficient computationally than the explicit method. Using a window graphics XGrafix[25] on a dedicated Pentium/120 with LINUX, a typical simulation takes 1–2 days for the two-dimensional code and 1/4–1/2 day for the one-dimensional code with XGrafix.

It is well known[21] that because of strong coupling between Poisson's equation and electron continuity equation, explicit methods with successive solutions of Poisson's equation and the continuity equations have a time step limited by $\tau_d = \epsilon_0/e(n_e\mu_e + n_p\mu_p) \approx \epsilon_0/en_e\mu_e$, that is, the dielectric relaxation time. We note that Fiala *et al.*[8] and Stewart *et al.*[21] employed different methods with time steps much larger than τ_d to overcome this problem. An improvement of our code along those lines is still feasible.

4. Two-Dimensional Fluid Simulation

Two-dimensional fluid simulations using the FL2D code[16,17] in a Cartesian (x, y) coordinate system are carried out for the system with two sources in a modified system of $11.5 \times 11\,\mathrm{cm}^2$ to reduce the computational cost. Figure 1 shows the eight-source system used in the experiment.[4] The third dimension, $z = 72.5\,\mathrm{cm}$ in the experiment, is considered to be infinitely long and thus is ignored in our approximate model in the two-dimensional simulation. Rectangular shapes of the sources are used to adapt to the Cartesian geometry used in the simulation. The inductive nature of the large-area plasma source is approximated in our simulation as the power deposition profile shown in Fig. 1(b) around the eight antennas imbedded in the plasma.

The typical two-dimensional simulation of two rectangular sources for a localized power deposition profile with a default value of a skin depth of 1.68 cm is shown in Fig. 2, where the steady-state profiles of the average electron density, the electron temperature, and the plasma potential are given. A gas pressure of 1 Torr and modified system size of 100 W/cm are used for the total power absorbed along the third dimension to be 7.25 kW. For such a high power, the capacitive as well as inductive effects become important, which is the subject of a future study. The power deposition has a profile described[18] by $P = P_0 \exp(-2x/\delta)$ with $\delta = (m_e/e^2\mu_0 n_{e0})^{1/2}$, and P_0, in units of $\mathrm{W{\cdot}cm^{-1}}$ is adjusted to yield the total power as prescribed in the input parameter. The initially uniform electron density of $10^9\,\mathrm{cm}^{-3}$ gives a uniform $\delta = 1.68\,\mathrm{cm}$ which yields the power deposition profile shown in Fig. 1(b) with eight antenna sources. The self-consistent calculation of the induced electric field used in ref. 7 was not employed in the present work and will be the subject of future work.

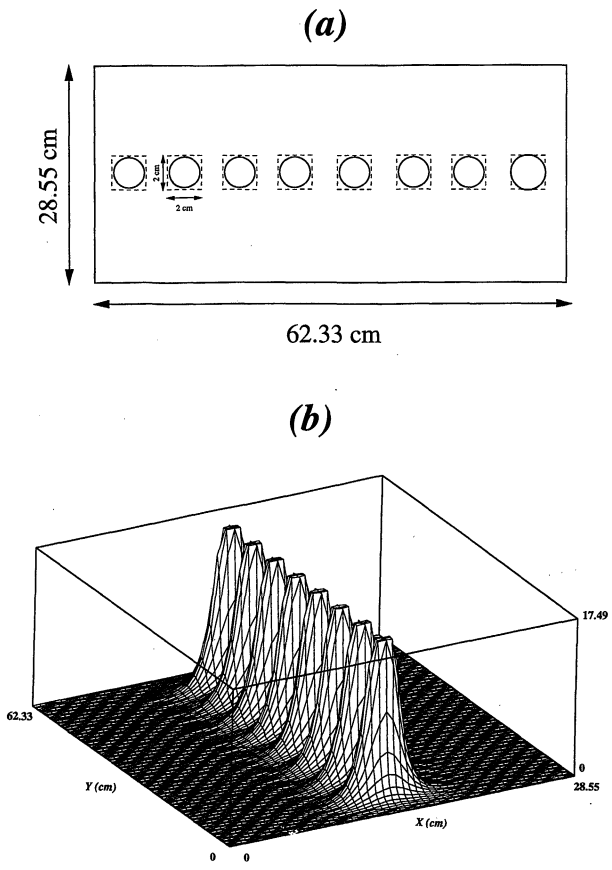

Fig. 1. The large-area plasma source. (a) Sideview with the third dimension in the experiment ignored. (b) Deposition profile of power (in unit of $\mathrm{W{\cdot}cm^{-1}}$) in the eight-source system.

The comparison with results of simulations using other parameters will be discussed in the following sections. A high gas pressure enables the use of a large time step due to the dielectric relaxation criterion.

The ratio of the electron density to the Boltzmann density, $R = n_e/\exp(V/T_e)$, is shown in Fig. 2(d). The units of R are the same as for the density, $10^9\,\mathrm{cm}^{-3}$. It exhibits a fairly uniform distribution, except in the sheath regions near the sources and the boundaries. Figures 2(e) and 2(f) show the profiles of ionization, calculated from the electron temperature using the appropriate argon cross-sectional data[18] and the ion current density at the substrate located at $x = 11\,\mathrm{cm}$ (3 cm from the source edge). The latter value reaches $5.0\,\mathrm{A/m^2}$ and is calculated using the ion velocity v_i at a location related to eq. (6). This v_i value is approximately eight times smaller than that calculated using the local Bohm velocity u_B. In the steady state, reached at approximately $30\,\mu\mathrm{s}$ with a time step of 5 ps, the average electron density and temperature are $2.94 \times 10^{11}\,\mathrm{cm}^{-3}$ and 1.46 V, respectively.

The profile uniformity along y, as shown in Fig. 2(f), can be improved by reducing the source separation, keeping the total power constant. The steady state at $18.6\,\mu\mathrm{s}$, shown in Fig. 3, exhibits substantial improvement in the uniformity while keeping the ion current density in a sim-

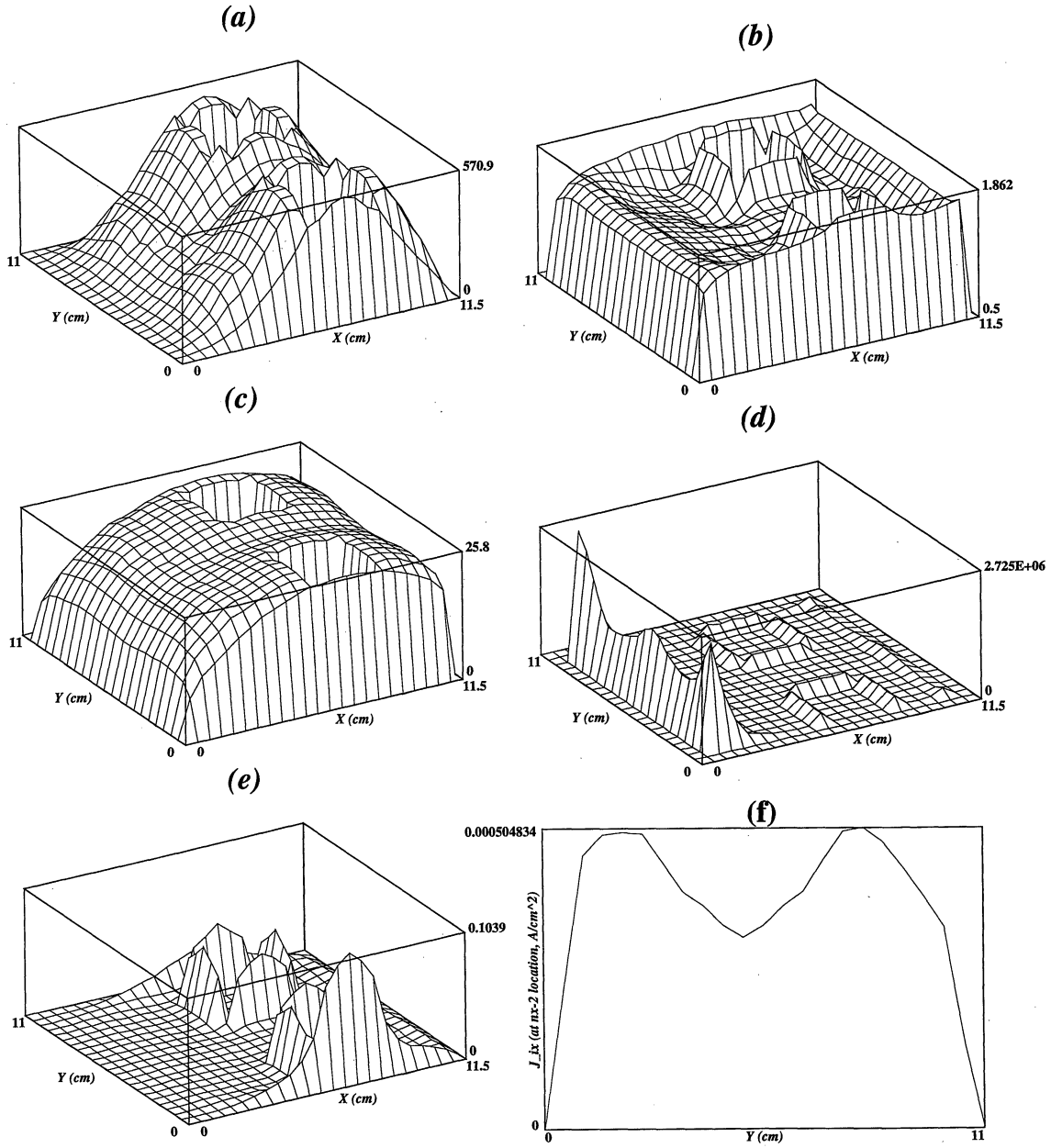

Fig. 2. The two-dimensional fluid simulation with two sources. (a) The electron density n_e in $10^9\,cm^{-3}$. (b) The electron temperature T_e in volts. (c) The plasma potential V in volts. (d) The Boltzmann ratio R in $10^9\,cm^{-3}$. (e) The ionization rate R_{iz} in $10^{18}\,cm^{-3}\cdot s^{-1}$. (f) The ion current density in the x-direction J_{ix} at the substrate.

ilar range ($6.3\,A/m^2$). The ion current density calculated from u_B (not from v_i) is $50.4\,A/m^2$. The average electron density and the temperature at the steady state are $2.93\times10^{11}\,cm^{-3}$ and 1.50 V, respectively. The source size is reduced to 1 cm rectangles as compared with 2 cm used in Fig. 2 and rods of 2 cm diameter in the experiment.

It is noted in Fig. 3(d) that the Boltzmann ratio R for this case is fairly uniform, except in the left boundary region where the true steady state takes more time due to low density and relatively high potential. For cases with an increased uniformity in the power deposition profile, this Boltzmann ratio becomes even more uniform. This enables the use of the Boltzmann relation in lieu of Poisson's equation when calculating the plasma potential. This replacement (thus, an approximation) of Poisson's equation was employed. This reduces the computation time by a factor of 10 to 100 owing to the reduced Courant (dielectric relaxation) condition, since the electric field is given by the Boltzmann relation, $\boldsymbol{E} = -kT_e\nabla n/n$ (not from the solution of Poisson's equation); therefore the strong coupling between Poisson's equation and the electron continuity equation is avoided. The approximate two-dimensional simulations at least enables an efficient comparison of results with various plasma parameters. The simulation with BOL-2D, namely, with the Boltzmann assumption at every time step for the case of Fig. 2, yields an average density ($2.50\times10^{11}\,cm^{-3}$), temperature (1.67 V), and ion current density from the Bohm velocity u_B ($40.0\,A/m^2$), which are similar to those in Fig. 2. However, the temperature profile is significantly different from that in Fig. 2. This limits the use of this model to a relative comparison in

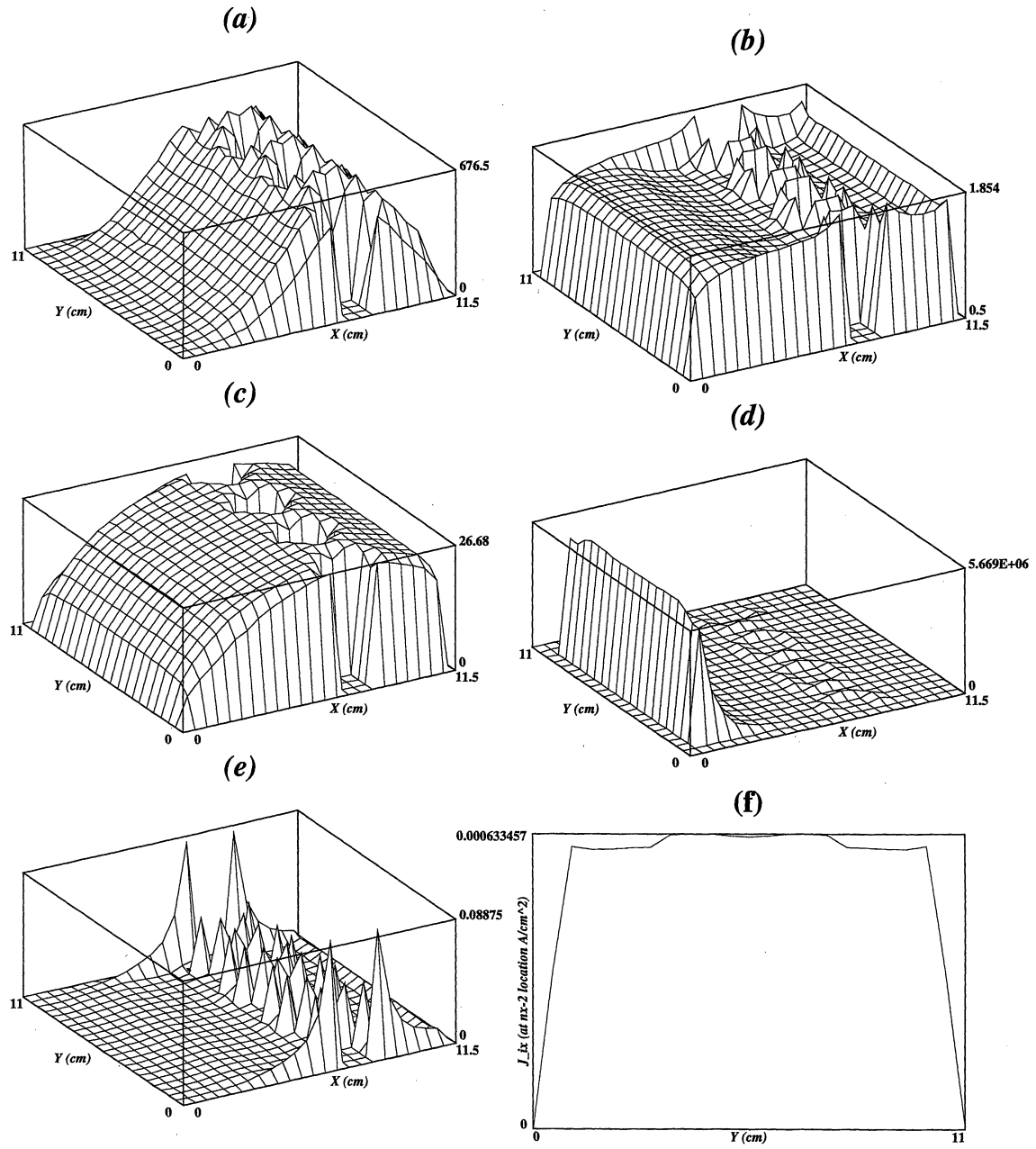

Fig. 3. The four-source simulation. (a) The electron density n_e in 10^9 cm^{-3}. (b) The electron temperature T_e in volts. (c) The potential V in volts. (d) The Boltzmann ratio R. (e) The electric field vectors $\boldsymbol{E}$. (f) The ion current density along x-direction, J_{ix}.

the optimization of plasma parameters or to cases with no embedded sources, such as a large-area plasma source, which contains no sheath region in the bulk plasma, with uniform deposition profiles.

In Fig. 4, the BOL-2D simulations with three different source types are compared, keeping the other plasma and numerical parameters the same. The use of a stretched source along the y-direction does not improve the uniformity of the ion current density from u_B, while the magnitude is enhanced to 310 A/m^2. The employment of more sources with reduced source separation significantly enhances the uniformity to 5%. The limiting cases of a continuous source along the y-direction are the subjects of the one-dimensional simulation described in the next section.

5. One-Dimensional Fluid Simulation

The one-dimensional fluid code employs the same equations as in the two-dimensional code. The source is continuous along the second ignorable coordinate y, as in Fig. 5(e), which shows the limiting case of Fig. 4(a). The one-dimensional fluid (FL1D) simulation for the case of Fig. 2 is shown in Fig. 5. The power density in the one-dimensional simulations is 9.09 W/cm^2, giving the total volume-integrated power of 7.25 kW when the two ignored dimensions of 11 cm and 72.5 cm are used. The average density and the temperature in the steady state (15.3 μs) are 2.85×10^{11} cm^{-3} and 1.52 V, respectively. These average values and the profiles in Fig. 5 are sufficiently close to those in Fig. 2 despite the difference

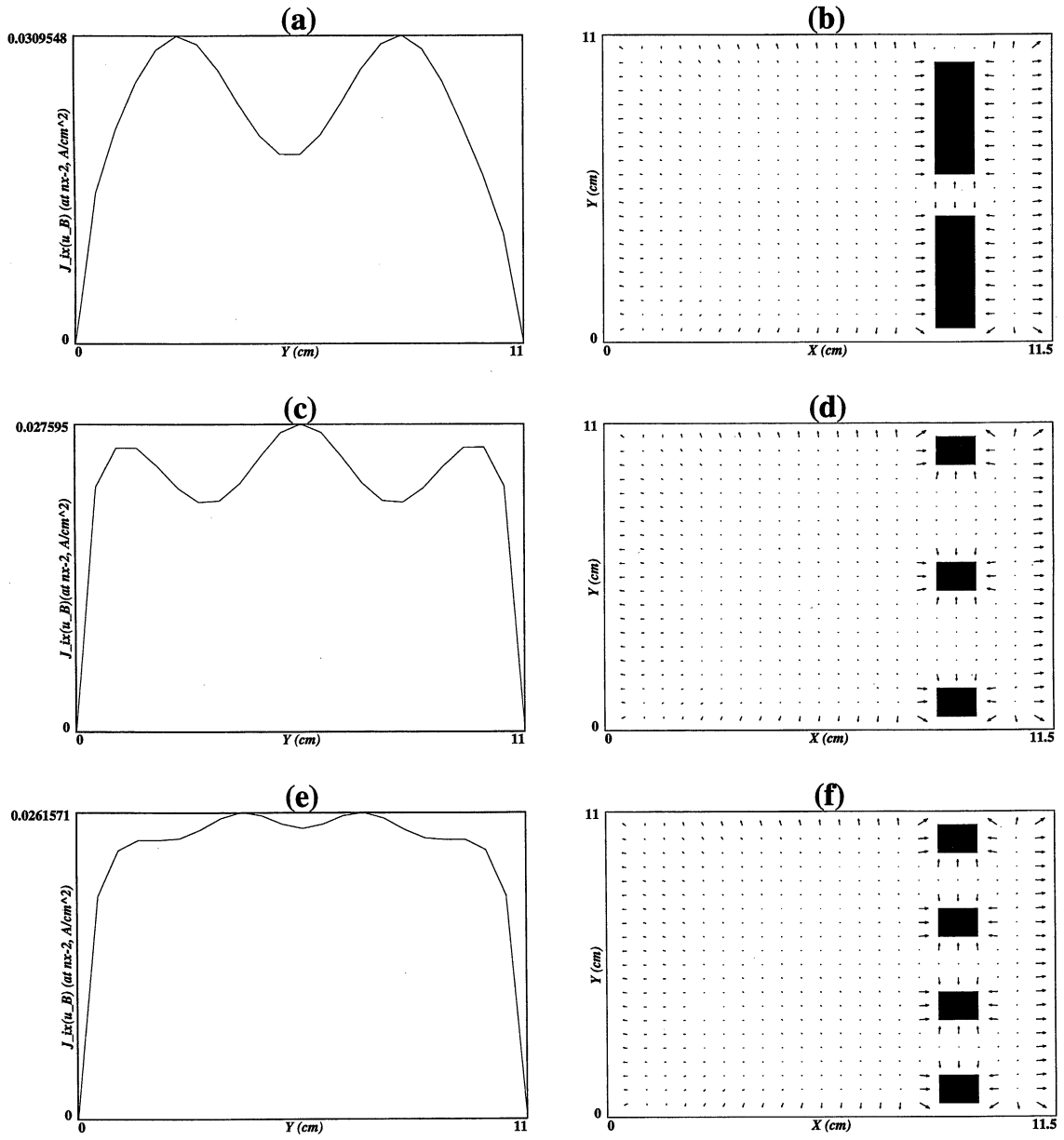

Fig. 4. The Boltzmann simulation for various source shapes. (a) The ion current density J_{ix} from u_B for the stretched source. (b) The electric field pattern for the stretched source. (c) J_{ix} for the three sources. (d) The electric field pattern for the three sources. (e) J_{ix} for the four sources. (f) The electric field pattern for the four sources.

in the source shape. The peak plasma potential of 25.6 V is close to the 25.8 V in Fig. 2. The ion current density measured at $x = 11$ cm with v_i (u_B) is 4.5 (36.8) A/m^2, similar to the case of Fig. 2. The Boltzmann ratio as in Fig. 5(d) is very uniform except at the left boundary at which more time is required to reach the steady state. The power deposition profile in Fig. 5(f) reflects the skin depth of 1.68 cm, and the system structure in Fig. 5(e) depicts the continuous source along the ignored y-dimension.

The usefulness of the one-dimensional fluid code is considerable in time-consuming simulations such as for fine-grid effects and low-gas-pressure cases. For fine spatial grids with $\Delta x = 1/4$ cm (1/2 of the Fig. 5 case), the FL1D simulation yields an average density of 2.79×10^{11} cm^{-3}, an average temperature of 1.52 V, and a peak potential of 27.7 V; these values are qualitatively the same as those for the coarser grid case. For 0.1 Torr, FL1D simulation with the same total power gives an average density of 1.24×10^{11} cm^{-3}, an average temperature of 2.11 V, the peak plasma potential of 39.0 V, and an ion current density of 80.5 A/m^2 in the steady state (at 1.8 μs). Results for other cases with smaller gas pressures are compared in Fig. 6 with those of the global model. The results of the global model compare reasonably well with those of the finite-dimensional fluid simulation.

The FL1D simulations with the skin depth changed from 1.68 cm to 3.36 cm (or to 6.72 cm) for the 1 Torr case yield the average density of 2.60×10^{11} cm^{-3} (or 2.89×10^{11} cm^{-3}), the average temperature of 1.59 V (or 1.15 V), the peak potential of 29.6 V (or 28.9 V), and the ion current density of 136 A/m^2 (or 109 A/m^2).

The steady-state profiles of the BOL-1D simulation can be used as the initial profiles in the full FL1D sim-

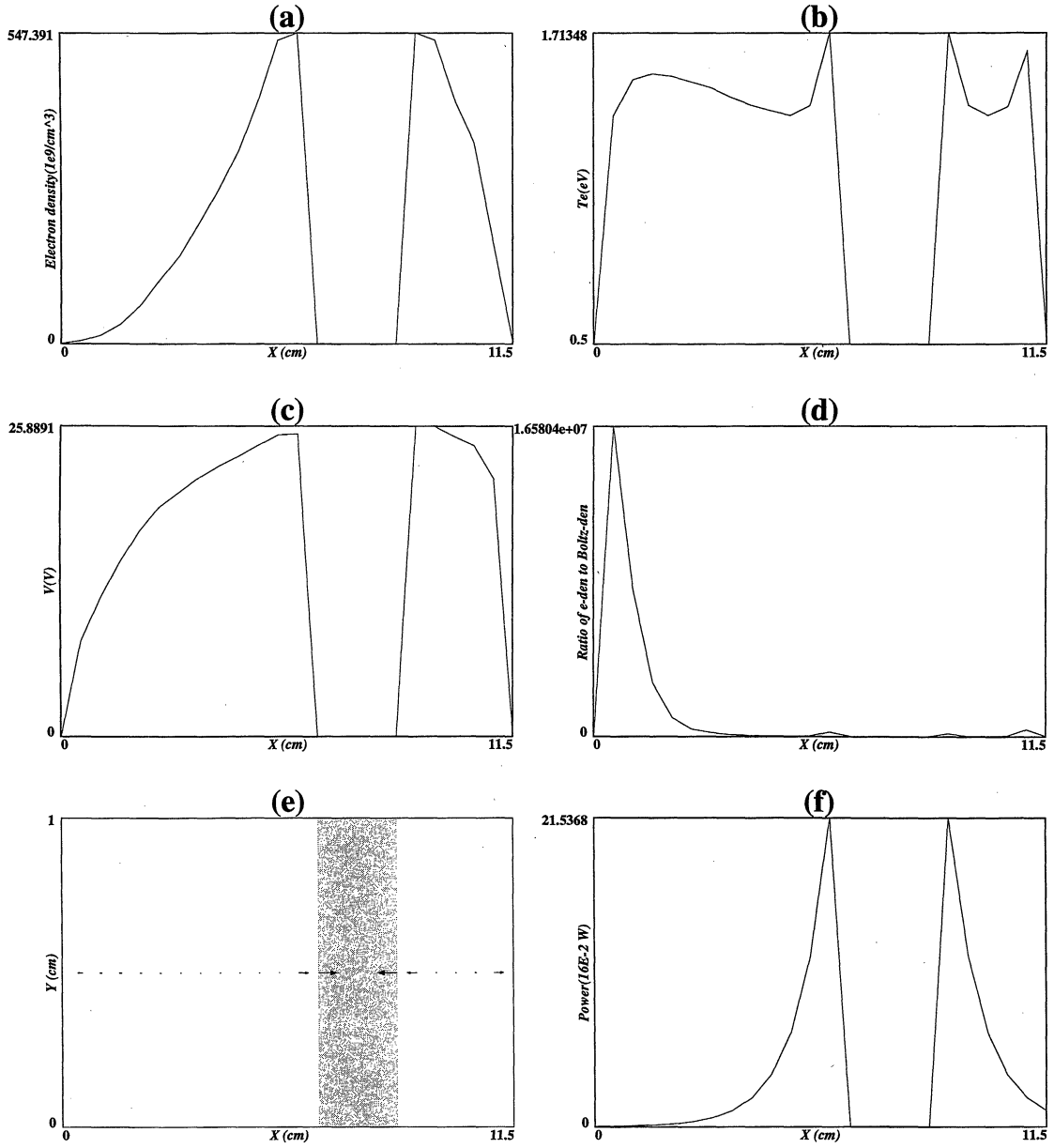

Fig. 5. The one-dimensional fluid simulation for the case of Fig. 2. (a)–(d) as in Fig. 3. (e) The electric field pattern. (f) The power deposition profile.

ulation which yield a final answer that is in agreement with that of the conventional FL1D simulation. This initial condition, however, shows a minimal gain in the total computation time. The pulsed power and the after-glow phenomenon are also examined and will be reported in a future paper.

6. Global Modeling

For global modeling, we use the electron continuity equation and the electron temperature equation without Poisson's equation, and no limitation from the dielectric relaxation constraint is required. The wall losses through the Cartesian boundaries are modeled in a fashion similar to the axial loss of the global model in a slab geometry.[26–28] The equations used are

$$\frac{\partial n_e}{\partial t} = -\frac{n_e u_B}{d_{eff}} + R_{iz} - \alpha n_e^2, \tag{18}$$

$$\frac{\partial}{\partial t}\left(\frac{3}{2}n_e k T_e\right) = P - P_{coll} - \frac{n_e u_B}{d_{eff}}\left(\frac{5}{2}kT_e + e|V_s|\right) - \alpha n_e^2 \frac{3}{2}kT_e, \tag{19}$$

$$d_{eff} = \frac{1}{2}\frac{X \times Y}{(X \times h_y + Y \times h_x)}, \tag{20}$$

$$h_1 = 0.86\left(3.0 + \frac{1}{2}\frac{X}{\lambda_i}\right)^{-\frac{1}{2}},\ h_2 = 0.86\left(3.0 + \frac{1}{2}\frac{Y}{\lambda_i}\right)^{-\frac{1}{2}},$$
$$h_x = h_1\frac{\sin(\cos^{-1}h_2)}{\cos^{-1}h_2},\ h_y = h_2\frac{\sin(\cos^{-1}h_1)}{\cos^{-1}h_1} \tag{21}$$

where d_{eff} is the effective plasma size and X and Y are the dimensions of the planar source. h_1 and h_2 are the ratios of the density at the sheath to the bulk density for the infinite slab, which were derived by Godyak.[26]

Assuming a cosine-shaped density profile, we used the

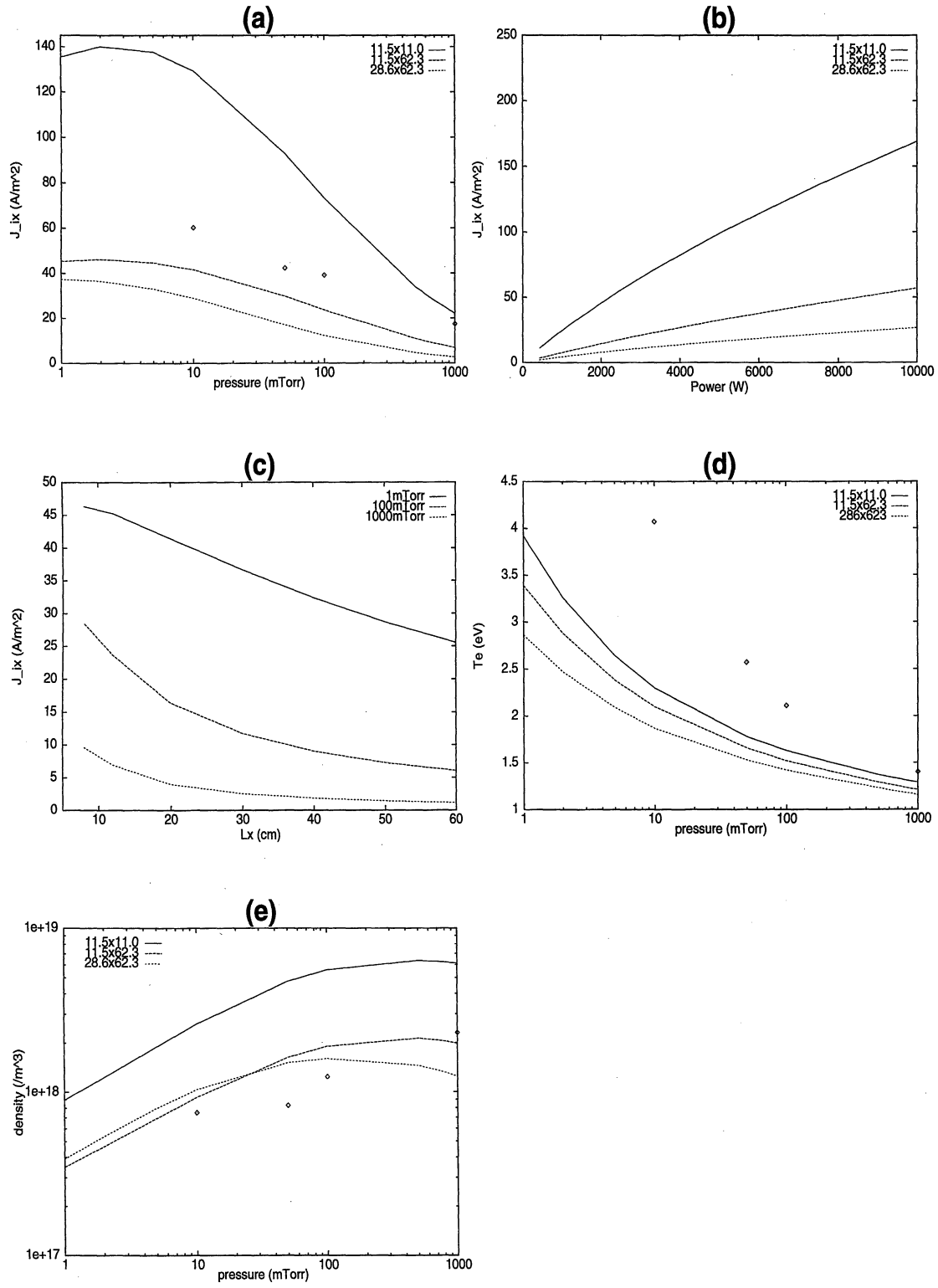

Fig. 6. The steady-state global model for the three system sizes. The diamonds are for FL1D simulation for the system size of $11.5 \times 11.0\,\mathrm{cm}^2$. (a) The ion current density J_{ix} vs gas pressure. (b) J_{ix} vs the total power. (c) J_{ix} vs the x-dimension which is adjustable in the experiment as shown in Fig. 1. (d) The average temperature vs the pressure. (e) The average density vs the pressure.

modified expressions for h_x and h_y which still have a possibility for further improvement for a finite-sized rectangular system such as the large-area plasma source. P is the volume density of the power absorbed in the system. λ_i is the ion mean-free path. V_s is the sheath voltage and $V_s \approx 4.7T_e$ for argon.

To obtain the steady state, we employed two methods, a time-independent solver and a time-dependent code, which are in excellent agreement with each other for a test case in cylindrical or Cartesian coordinates. For the uniform deposition of power, the agreement between global modeling and the two-dimensional fluid simulation is better than that for localized deposition. For the latter case, the agreement is qualitative but still rea-

sonably fair, considering the localized profiles as in the skin depth of 1.68 cm. The typical time evolutions of the time-dependent global simulations for several gas pressures reach the steady state in approximately 1 ms. This time-dependent global simulation requires a substantial computing time to obtain the steady-state values. The steady-state solver requires virtually no significant computing. The equations are

$$\alpha n_e = N K_{iz} - \frac{u_B}{d_{eff}}, \tag{22}$$

$$0 = P - P_{coll} - \frac{n_e u_B}{d_{eff}} \left(\frac{5}{2} k T_e + e|V_s| \right) - \alpha n_e^2 \frac{3}{2} k T_e. \tag{23}$$

Substituting the first equation for n_e as a function of T_e into the second equation, we have a nonlinear equation for T_e as a function of the input power density P, which is solved by using the Müller method.[29] The global calculations, both the steady-state solver and the time-dependent simulation, produce identical results with agreement up to the 4th or 5th significant digits. The global results also agree with those of FL2D and FL1D simulation for the cylindrical case in which we derived a hybrid code by combining the two codes.

The ion current densities, electron densities, and electron temperatures calculated from the steady-state solver are shown in Fig. 6 versus gas pressure, total power, and system size. For the system size of $11.5 \times 11\,cm^2$ used in the two-dimensional fluid simulations, the ion current density at a gas pressure of 10 (1000) mTorr reaches 130 (30) A/m^2. For the experimental system of $28.6 \times 62.3\,cm^2$, it changes to 30 (5) A/m^2, as shown in Fig. 6. The total power absorbed along the third dimension of 72.5 cm is assumed to be 2.5 kW, as in the experiment. The effect of varying the separation L_x between the top and the bottom substrates is shown in Fig. 6(c). These values from the global model for the large-area plasma source show the best agreement with those from a finite-dimensional (1-D or 2-D) fluid simulation of a uniform deposition profile. Since most of the experimental cases correspond to a localized deposition profile with $\delta \sim 1.68$ cm, the global results should be considered to represent the upper limits of the plasma density and the ion current density; these are in fact observed in Fig. 6.

7. Summary and Conclusion

Large-area plasma discharges are simulated based on two-dimensional as well as one-dimensional fluid models in Cartesian geometry. The profile distributions of charged particles, electron temperature, and electric field are examined.

The large-area plasma source simulated shows plasma parameters similar to those of a transformer-coupled plasma source. The major difference is in the source shape and the wall loss at the source location. Employing a properly optimized source shape, the simulation results of the large-area plasma source at a hypothetical gas pressure (in the range of 0.1 Torr which is higher than 0.01 Torr in the experiment because of the computational effectiveness of the simulation) and a high power (7.5 kW) provide a high average plasma density (in the range of $10^{12}\,cm^{-3}$), a low average electron temperature (in the range of 2 V), and the ion current density at the substrate location, 1.5–3.0 cm from the source edge (in the range of $40\,A/m^2$). These parameters are obtained with good uniformity.

The simulated results for the large-area plasma source show that the electron temperature becomes more uniform than the plasma potential and the electron density. The latter forms a very peaked profile localized near the driving sources. The boundary condition at the wall makes the density zero, but away from the antenna wall, the power deposition profile, as shown in Fig. 1(b), produces a peaked density profile near the antenna regions. The peaked profile gradually spreads away from the antenna via various collision processes.

When the one-dimensional and two-dimensional fluid simulations are computationally demanding, the approximate global model is used. The profile information obtained from the multi-dimensional simulations and the average quantities calculated using the global model can provide useful information in the projection of the steady plasma density and ion current density at the substrate.

The validity of the Boltzmann relation, which is widely used in many analyses, is examined and found to be reasonable in the plasma bulk region, except in the sheaths or for low-pressure cases. A simulation code using the Boltzmann assumption is utilized to determine the optimal parameters for many time-consuming cases.

Acknowledgements

Helpful suggestions from Professor M. A. Lieberman and the sabbatical term with Professor C. K. Birdsall's group during 1995 by one of the authors (JKL) are gratefully acknowledged.

This work is supported in part by the Basic Science Research Institute Program, Ministry of Education (BSRI-95 and 96-2439).

1) M. A. Lieberman and A. J. Lichtenberg: *Principles of Plasma Discharges and Materials Processing* (Wiley, New York, 1994).
2) Y. P. Raizer: *Gas Discharge Physics* (Spring-Verlag, Berlin, 1991).
3) D. B. Graves: IEEE Trans. Plasma Sci. **22** (1994) 31.
4) Y. Wu and M. A. Lieberman: UCB/ERL Memo M95/60 (1995).
5) V. P. Gopinath and M. A. Lieberman: UCB/ERL Memo M95/65 (1995).
6) G. G. Lister: J. Phys. D **25** (1992) 1649.
7) P. Ventzek, R. J. Hoekstra and M. J. Kushner: J. Vac. Sci. Technol. B **12** (1994) 461.
8) A. Fiala, L. C. Pitchford and J. P. Boeuf: Phys. Rev. E **49** (1994) 5607.
9) F. F. Young and C. H. Wu: IEEE Trans. Plasma Sci. **21** (1993) 312.
10) D. B. Graves and K. F. Jensen: IEEE Trans. Plasma Sci. **14** (1986) 78.
11) J. P. Boeuf and L. C. Pitchford: IEEE Trans. Plasma Sci. **19** (1991) 286.
12) G. DiPeso, T. D. Rognlien, V. Vahedi and D. W. Hewett: IEEE Trans. Plasma Sci. **23** (1995) 550.
13) M. Li, H. M. Wu and Y. Chen: IEEE Trans. Plasma Sci. **23**

(1995) 558.
14) W. J. Goedheer, P. M. Meijer, J. Bezemer, J.D.P. Passchier and W. G. van Sark: IEEE Trans. Plasma Sci. **23** (1995) 644.
15) S. K. Park and D. J. Economou: J. Appl. Phys. **68** (1990) 3904.
16) J. K. Lee, L. Meng, H. Lee, Y. Lim, B. K. Kang and T. H. Chung: Bull. Am. Phys. Soc. **40** (1995) 1773.
17) J. K. Lee *et al.*: IEEE-ICOPS, Boston, 1996, p. 165.
18) R. A. Stewart, P. Vitello, D. B. Graves, E. F. Jaeger and L. A. Berry: Plasma Sources Sci. Technol. **4** (1995) 36.
19) A. P. Paranjpe: J. Vac. Sci. Technol. A **12** (1994) 1221.
20) T. Intrator and J. Menard: Plasma Sources Sci. Technol. **5** (1996) 371.
21) R. A. Stewart, P. Vitello and D. B. Graves: J. Vac. Sci. Technol. B **12** (1994) 478.
22) J. D. P. Passchier and W. J. Goedheer: J. Appl. Phys. **74** (1993) 3744.
23) A. L. Ward: J. Appl. Phys. **33** (1962) 2789.
24) D. L. Sharfetter and H. K. Gummel: IEEE Trans. Electron Devices **16** (1967) 64.
25) V. Vahedi P. Mirrashidi, D. K. Wong and J. Verboncoeur: XGrafix (version 2.01), (c) Copyright 1991–1995 The Regents of the University of California.
26) V. Godyak: *Soviet rf Discharge Research* (Delphic Associates, Falls Church, VA, 1986).
27) H. J. Lee and J. K. Lee: Jpn. J. Appl. Phys. **35** (1996) 6252.
28) T. H. Chung, S. H. Lee and J. K. Lee: Ungyong Mulli **10** (1997) 40 [in Korean].
29) W. H. Press, B. Flannery, S. Teukolsky and W. Vetterling: *Numerical Recipes in C* (Cambridge University Press, New York, 1988).